ORIGINAL PAPER

Yinghui Zhu · J. Woody Ju

Interface energy effect on effective elastic moduli of spheroidal particle-reinforced nanocomposites

Abstract By incorporating the interface energy effect into a classical micromechanics framework, effective elastic moduli of a composite material containing randomly distributed nanosized prolate spheroidal inhomogeneities are investigated in this paper. The effect of interface energy, which is usually neglected in classical micromechanics theories, becomes important when the size of the reinforcement phase in the composite enters the nanometer range. The interface energy effect is simulated by inducing interface stress on the zero-thickness membrane interface between the matrix and the inhomogeneities. The interfacial stress discontinuity equations are formulated in accordance with the equilibrium conditions on the idealized interface, from which the interfacial strain discontinuity is solved. Subsequently, the effective elastic moduli are derived based on the classical micromechanics homogenization approaches. Comparisons are made of the effective moduli under the current nanomechanical framework and under classical micromechanical theory. The effective moduli are shown to be dependent upon the size of the inhomogeneities and the interface properties when the interface energy effect is considered.

1 Introduction

The advancement of material science in nanotechnology provides new insights into particles in nanoscale and has attracted considerable attention in a wide range of disciplines such as astronomy, medicine, electronics, optics, etc. [1]. Nanoparticles, having one or more dimensions in nanometer scale, may possess desirable properties different from conventional materials due to their greater specific surface areas. Currently, scientists attempt to use nanoparticles as the reinforcement phase in composite materials to create new materials with improved properties, such as high strengths, high moduli, high heat resistance, low gas permeability and low flammability [2,3]. Meanwhile, predictions on the mechanical properties of nanocomposites have drawn significant attention. As nanocomposites are heterogeneous materials consisting of phases with distinctive properties and length scales, it is impractical to find the point-wise mechanical properties of a random material point. Instead, a common practice is to consider the overall effective properties of a heterogeneous composite. For composites with large-sized reinforcement (typically in the micrometer or larger scale), classical micromechanics theories have exhibited good predictions on the effective mechanical properties; e.g., the direct Eshelby method [4–6] for dilute particle concentration, the Mori–Tanaka method [7,8] for moderate concentration, and the pairwise particle interaction model [9,10] for moderately high particle concentration. In this paper, the homogenization scheme of the classical micromechanics theory, the Mori–Tanaka method or

Y. Zhu · J. W. Ju (✉)
Department of Civil and Environmental Engineering, University of California, Los Angeles, CA 90095-1593, USA
E-mail: juj@ucla.edu

Y. Zhu
E-mail: zhuyinghui@g.ucla.edu

the first-order non-interacting method [7,8], is incorporated into the determination of the effective properties of nanocomposites.

It is well known that the local atomic environment at the particle–matrix interface is different from its setting associated with the interior. As a consequence, the free energies possessed by the molecules at the particle–matrix interface and by the molecules in the interior are different. Gibbs, who first pointed out this phenomenon in 1906, proposed the concept of interface energy as the excess free energy per unit area of the interface [11]. As the mechanical properties of a solid are related to its associated free energy, they are affected by the interface energy at the interface [12]. In classical micromechanics theories, the effect of interface energy is neglected because of the relatively low specific interface area as well as the small gross interface area in the composite. However, when one or more dimensions of a solid phase is (are) in nanoscale, the interface energy becomes one of the main factors that determine the material properties of a composite including its mechanical performances [13]. For a nanocomposite, since the dimensions of the inhomogeneities are in the nanometer scale, the effect of interface energy needs to be considered. To characterize the interface energy effect on the mechanical properties, several models are proposed in the literature; among them, the interphase model and the interface model are most widely discussed. The interphase model [14–17] assumes that there exists a layer between the matrix and an inhomogeneity, which is referred to as the interphase. The interphase transfers the load from the matrix to an inhomogeneity, and it can be regarded as a separate phase with a specified thickness and mechanical properties. On the other hand, the interface model, originating from the classical treatments for the imperfect bonding conditions in composite materials, assumes discontinuous stress and/or displacement from the matrix to an inhomogeneity; e.g., the free tangential interface sliding in the free sliding model, the linear displacement–traction relation in the linear spring model, and the linear relationship between the displacements on the two sides of the interface in the dislocation-like model [18].

In the study of capillarity, the interface energy is shown to be equal to the surface tension (the interface stress) *numerically* under certain occasions, and they are often wrongly regarded as equivalent [19]. However, Gibbs [11] distinguished these two concepts by the thermodynamics approach. He defined the interface stress as the reversible work required to elastically stretch an existing interface. In order to study the mechanical behavior of material surfaces, Gurtin and Murdoch [20] established a mathematical framework for the material surfaces following the continuum mechanics theory. The formulation is based on the interphase model, in which the thickness of the interphase is set to be *zero*. As a consequence, the membrane theory applies, and only in-plane forces are retained in the idealized zero-thickness interphase. According to the elastic theory of membranes, Gurtin and Murdoch [20] assumed continuous displacements but discontinuous stress at the interface by inducing the in-plane interface stress. The corresponding interface boundary conditions, which involve the interface stress terms, are named the *generalized* Young–Laplace equations, as a counterpart of the well-known Young–Laplace equations in fluid mechanics. The *generalized* Young–Laplace equations can be expressed as:

$$[\boldsymbol{\sigma}] \cdot \mathbf{n} = -\boldsymbol{\nabla}_S \cdot \boldsymbol{\tau}, \tag{1}$$

where $[\boldsymbol{\sigma}]$ denotes the difference of stress at the interface between the matrix and the reinforcement, $\mathbf{n}$ is the outward unit normal to the interface, and $-\boldsymbol{\nabla}_S \cdot \boldsymbol{\tau}$ is the surface divergence of the interface stress $\boldsymbol{\tau}$. In the following expressions, $[\cdot]$ represents the discontinuity of said value at the interface from the matrix to the inhomogeneity. From the *generalized* Young–Laplace equations, relations of the elastic fields at the interface between the matrix and the inhomogeneity can be determined.

Recently, some researchers have studied the mechanical properties of nanostructured elements, such as nanosized plates and beams [21], spherical nanoparticles, thin films and nanowires [22,23]. However, only a few researchers focus on the effective mechanical properties of nanocomposites, and experimental data are especially rare in the literature. Sharma et al. [24] included the interface energy in the total free energy and rendered a variational formulation to determine the stress and the strain states for the composite containing a single spherical nanoinclusion, in which dilatational eigenstrain is assumed. Sharma and Ganti [25] proposed a revised size-dependent Eshelby tensor that considers the interface energy effect and presented its expressions for spherical and cylindrical inclusions with dilatational eigenstrain. Duan et al. [12] addressed the spherical nanoinhomogeneity problem and predicted the effective moduli of the nanocomposite. Kushch et al. [26,27] employed the representative unite cell (RUC) model to consider the interactions of inhomogeneities in nanocomposites. Apart from considering the interface energy effect, the higher-order elasticity theories, including the couple stress theory and the micropolar theory, are also applied to consider the size effect in nanocomposites. By introducing the extra degree of freedom for local rotations of material points, the *material characteristic lengths* are considered in the corresponding governing equations in the higher-order theories, from which the size dependency is included. Shodja and Hashemian [28] adopted the couple stress theory

to consider the size effect in nanocomposites. Alemi and Shodja [29] predict the shear modulus of multi-coated elliptical fiber-reinforced nanocomposites through the micropolar theory. In addition to the research on the elastic behavior, the performances of nanocomposites under plastic deformation and damage are discussed [30–33]. Nevertheless, most of the existing approaches tackle the nanocomposite with spherical or cylindrical reinforcements, and studies on more general and more sophisticated spheroidal particle-reinforced nanocomposites are in demand.

In this paper, an analytical framework is proposed to predict the effective elastic moduli of prolate spheroidal particle-reinforced nanocomposites. The present framework is based on the classical micromechanics theories and considers the interface energy effect. At variance from the conventional perfect interface boundary conditions, which are assumed in micromechanics theories, the *generalized* Young–Laplace equations are incorporated at the interface to account for the interface energy-induced interfacial discontinuities. The interfacial strain discontinuity is solved for spheroidal particles. Further, effective moduli are derived following the homogenization approach in the Mori–Tanaka method. Compared with the classical micromechanical solutions on the effective moduli, the results are demonstrated to be dependent upon the size of the reinforcement particles and the properties of the interface.

2 Interface discontinuity conditions for spheroids

Following Gurtin and Murdoch [20], the interface energy effect is simulated by the *generalized* Young–Laplace equations. For a prolate spheroidal particle, we have

$$\frac{r^2}{b^2} + \frac{z^2}{a^2} = 1, \quad 0 \le \phi \le 2\pi, a > b. \tag{2}$$

The *generalized* Young–Laplace equations are [34]

$$[\sigma_{31}] = -\frac{1}{h_1 h_2} \left(h_2 \frac{\partial \tau_{11}}{\partial \phi} + \frac{\partial h_2}{\partial z} (\tau_{12} + \tau_{21}) + h_1 \frac{\partial \tau_{21}}{\partial z} \right), \tag{3}$$

$$[\sigma_{32}] = -\frac{1}{h_1 h_2} \left(h_2 \frac{\partial \tau_{12}}{\partial \phi} + \frac{\partial h_1}{\partial z} (-\tau_{11} + \tau_{22}) + h_2 \frac{\partial \tau_{22}}{\partial z} \right), \tag{4}$$

$$[\sigma_{33}] = -\left(\frac{\tau_{11}}{R_1} + \frac{\tau_{22}}{R_2} \right), \tag{5}$$

where $h_1 = r$, $h_2 = \sec \alpha$, $\alpha = \tan^{-1}\left(\frac{dr}{dz}\right)$, and $R_1 = -b\left(1 + \frac{z^2}{a^2}\left(\frac{b^2}{a^2} - 1\right)\right)^{1/2}$, $R_2 = -\frac{a^2}{b}\left(1 + \frac{z^2}{a^2}\left(\frac{b^2}{a^2} - 1\right)\right)^{3/2}$.

The interface energy is associated with the interfacial atomic environment. When the effect of interface energy is simulated by the interface stress, it is essential to determine the relation between the interface stress and the strain at the interface, which illustrates the change of the interfacial local atomic environment. Under the assumption of small deformation, a linearized constitutive relation has been widely employed in the literature [12,18,35]. When the interface of a particle in the composite material is considered, the linearized constitutive equation can be written as

$$\boldsymbol{\tau} = \mathbf{C}^{\mathrm{S}} : \boldsymbol{\varepsilon}^{\mathrm{S}}, \tag{6}$$

where $\mathbf{C}^{\mathrm{S}}$ is the interface elastic stiffness tensor and $\boldsymbol{\varepsilon}^{\mathrm{S}}$ is the interface strain. As the thickness of the idealized interphase is neglected, the interface strain becomes identical to the tangential components of the strain at the interface in the bulk material. As indicated by Duan et al. [12] that an isotropic interface is able to describe the interfacial elastic behaviors under small deformations, a linear isotropic constitutive relation is adopted here. The linear isotropic interface stiffness tensor follows the form

$$\mathbf{C}^{\mathrm{S}} = 2K^{\mathrm{S}} \mathbf{L}^{\mathrm{v}}_{ijkl} + 2\mu^{\mathrm{S}} \mathbf{L}^{\mathrm{d}}_{ijkl}, \tag{7}$$

for $i, j, k, l = 1, 2$, with

$$\mathbf{L}^{\mathrm{v}}_{ijkl} = \frac{1}{2} \delta_{ij} \delta_{kl} \mathbf{e}_i \otimes \mathbf{e}_j \otimes \mathbf{e}_k \otimes \mathbf{e}_l, \tag{8}$$

$$\mathbf{L}^d_{ijkl} = \frac{1}{2}\left(\delta_{ik}\delta_{jl} + \delta_{jk}\delta_{il} - \delta_{ij}\delta_{kl}\right)\mathbf{e}_i \otimes \mathbf{e}_j \otimes \mathbf{e}_k \otimes \mathbf{e}_l, \tag{9}$$

where K^S and μ^S are the 'bulk modulus' and the 'shear modulus' of the idealized two-dimensional interface. Numerical simulations and theoretical studies on the interface elastic properties were conducted in the recent literature. Miller and Shenoy [21], Mi et al. [36], Pahlevani and Shodja [37], and Shodja and Pahlevani [38] presented the molecular dynamics approach to determine the interface elastic constants of fcc crystals. Further, Shodja and Enzevaee [39] developed a theoretical approach utilizing ab initio DFT calculations to obtain the interface residual stress and the interface elastic constants of the (1 0 0) planes of fcc crystals. It is noted that although the interface residual stress perturbs the elastic fields *near* the interface, the change of the elastic fields due to the far-field loading are not influenced by the residual fields when elastic deformation is considered. Therefore, it is a common practice to neglect the effect of the interface residual stress on the effective elastic properties [12,40].

3 Interface discontinuities

For a single ellipsoidal particle-reinforced composite subjected to the far-field stress, the stress disturbance from the inhomogeneity is equivalent to the stress disturbance induced by a uniform stress-free strain (eigenstrain) in an inclusion [4,5,41,42]. On the other hand, for the multi-particle-reinforced composite, the particle–particle and the particle–matrix interactions are much more complicated compared with the single particle composite, which lead to nonuniform elastic fields surrounding each particle and nonuniform eigenstrain in the equivalent inclusions. To simplify the interaction problem, an effective medium approach was suggested by Mori and Tanaka [7] (cf. Ju and Chen [9,10]) to treat each particle as a single particle inside an effective matrix, which expands the use of Eshelby's formulation to the multi-particle case and enables the prediction of effective properties. The Mori–Tanaka method is essentially a special case of the particle interaction framework proposed by Ju and Chen [9,10], if the first-order non-interacting method is adopted. However, the perfect interface conditions (the continuous stress and strain through the interface) are assumed in the Eshelby's framework. When discontinuities are introduced at the interface, we use the *generalized* Young–Laplace equations to determine the stress and the strain fields in the reinforcement particles instead of the Eshelby's solutions.

Now we consider a multi-phase prolate spheroidal particle-reinforced nanocomposite with isotropic reinforcements and the matrix material. Let us assume that all particles are unidirectionally aligned, and the particles in each reinforcement phase are identically shaped and randomly distributed in the matrix. When the particles are not unidirectionally aligned, the present work can be easily generalized with specified orientation distribution. For the rth phase particle Ω_r, let us follow Mori and Tanaka's assumption by regarding each particle as a single particle embedded in an otherwise homogeneous effective matrix with the averaged strain $\bar{\boldsymbol{\varepsilon}}_0$. Further, the averaged strain is also considered in the particle for simplicity. Following the equivalent inclusion principle, the equivalent inclusion equation for Ω_r can be rendered as

$$\mathbf{C}_0 : \left(\boldsymbol{\varepsilon}_r - \boldsymbol{\varepsilon}_r^*\right) = \mathbf{C}_r : \boldsymbol{\varepsilon}_r, \tag{10}$$

where $\mathbf{C}_0$ and $\mathbf{C}_r$ are, respectively, the stiffness tensor of the matrix and the particle, $\boldsymbol{\varepsilon}_r$ is the averaged total strain in the particle, and $\boldsymbol{\varepsilon}_r^*$ is the eigenstrain. From Eq. (10), we have

$$\boldsymbol{\varepsilon}_r^* = \mathbf{D}_r^{-1} : \boldsymbol{\varepsilon}_r, \tag{11}$$

where

$$\mathbf{D}_r = (\mathbf{C}_r - \mathbf{C}_0)^{-1} : \mathbf{C}_0. \tag{12}$$

Furthermore, the elastic strain $\mathbf{e}_r$ in the particle becomes

$$\mathbf{e}_r = \boldsymbol{\varepsilon}_r - \boldsymbol{\varepsilon}_r^* = \left(\mathbf{I} - \mathbf{D}_r^{-1}\right) : \boldsymbol{\varepsilon}_r. \tag{13}$$

It is emphasized that the eigenstrain is *nonzero* in the particle domain and *zero* in the matrix domain and can be determined from Eq. (11) once the total strain of the particle is obtained.

Based on the assumption that no interfacial debonding happens at the matrix–reinforcement interface, the displacement continuity condition at the interface can be expressed as

$$[\mathbf{u}_r] = \mathbf{0}, \tag{14}$$

where $[\mathbf{u}_r]$ is the relative displacement at the interface between the surrounding matrix and Ω_r. From this point, $[\cdot]$ denotes the interfacial discontinuity of inner value from the matrix to the particle. It follows from Eq. (14) that the displacement gradient at the interface can be discontinuous over the interface [41,42], that is, we have

$$[\mathbf{u}_r \nabla] = \boldsymbol{\lambda}_r \otimes \mathbf{n}, \tag{15}$$

where $\boldsymbol{\lambda}_r$ is the vector that magnifies the discontinuity of the displacement gradient over the interface and $\mathbf{n}$ is the unit normal vector to the interface. It is noted that the discontinuity is along the normal direction to the interface, and the displacement gradient is continuous in the tangential direction. By substituting Eq. (15) into the strain compatibility equations, the interfacial strain discontinuity is rendered as

$$\boldsymbol{\varepsilon}_r^\lambda = [\boldsymbol{\varepsilon}_r] = \frac{1}{2}\left([\mathbf{u}_r \nabla] + [\nabla \mathbf{u}_r]\right) = \frac{1}{2}\left(\boldsymbol{\lambda}_r \otimes \mathbf{n} + \mathbf{n} \otimes \boldsymbol{\lambda}_r\right), \tag{16}$$

where $\boldsymbol{\varepsilon}_r^\lambda$ is defined as the strain discontinuity through the interface. In accordance with Eqs. (13) and (16), the interface discontinuity of elastic strain becomes

$$[\mathbf{e}_r] = [\boldsymbol{\varepsilon}_r] - \left[\boldsymbol{\varepsilon}_r^*\right] = \boldsymbol{\varepsilon}_r^\lambda + \boldsymbol{\varepsilon}_r^*. \tag{17}$$

Further, the interfacial stress discontinuity takes the form

$$[\boldsymbol{\sigma}_r] = \mathbf{C}_0 : [\mathbf{e}_r] = \mathbf{C}_0 : \left(\boldsymbol{\lambda}_r \otimes \mathbf{n} + \boldsymbol{\varepsilon}_r^*\right). \tag{18}$$

Substitution of Eqs. (6) and (18) into Eq. (1) leads to

$$\mathbf{C}_0 : \left(\boldsymbol{\lambda}_r \otimes \mathbf{n} + \boldsymbol{\varepsilon}_r^*\right) \cdot \mathbf{n} = -\nabla_{\mathrm{S}} \cdot \left(\mathbf{C}_r^{\mathrm{S}} : \boldsymbol{\varepsilon}_r^{\mathrm{S}}\right). \tag{19}$$

From Eq. (19), the vector of discontinuity $\boldsymbol{\lambda}_r$ can be determined by the eigenstrain $\boldsymbol{\varepsilon}_r^*$ in the particle and the total strain $\bar{\boldsymbol{\varepsilon}}_0$ in the matrix, whose tangential components are identical to the interface strain $\boldsymbol{\varepsilon}_r^{\mathrm{S}}$. Moreover, the strain discontinuity $\boldsymbol{\varepsilon}_r^\lambda$ can be solved according to Eq. (16). To determine the averaged strain in the particle, an interface averaging procedure is applied to the strain discontinuity $\boldsymbol{\varepsilon}_r^\lambda$:

$$\bar{\boldsymbol{\varepsilon}}_r^\lambda = \frac{1}{\partial \Omega_r} \int_{\partial \Omega_r} \boldsymbol{\varepsilon}_r^\lambda \mathrm{d}A = \mathbf{A}_r : \bar{\boldsymbol{\varepsilon}}_0 + \mathbf{B} : \boldsymbol{\varepsilon}_r^*, \tag{20}$$

where $\bar{\boldsymbol{\varepsilon}}_r^\lambda$ is the averaged interfacial strain discontinuity tensor, $\partial \Omega_r$ is the interface area of the particle Ω_r, and $\mathbf{A}_r$ and $\mathbf{B}$ are the coefficient tensors, whose detailed expressions are exhibited in Appendices 1 and 2 for prolate spheroids.

The coefficient tensors $\mathbf{A}_r$ and $\mathbf{B}$ are derived by considering the continuity conditions through the interface. For illustration, the detailed expressions of $\mathbf{A}_r$ and $\mathbf{B}$ under two limiting conditions are rendered here. When the spheroid reduces to a sphere with the radius a, the coefficient tensors $\mathbf{A}_r$ and $\mathbf{B}$ become isotropic tensors taking the forms

$$(A_r)_{ijkl} = \frac{1}{a}\left(\frac{8}{15}\frac{K_r^{\mathrm{S}}}{M_0} - \frac{2}{15}\frac{K_r^{\mathrm{S}}}{\mu_0} - \frac{4}{15}\frac{\mu_r^{\mathrm{S}}}{\mu_0}\right)\delta_{ij}\delta_{kl} + \frac{1}{a}\left(-\frac{4}{15}\frac{K_r^{\mathrm{S}}}{M_0} + \frac{2}{5}\frac{K_r^{\mathrm{S}}}{\mu_0} + \frac{4}{5}\frac{\mu_r^{\mathrm{S}}}{\mu_0}\right)\left(\delta_{ik}\delta_{jl} + \delta_{il}\delta_{jk}\right), \tag{21}$$

$$B_{ijkl} = \left(-\frac{1}{3}\frac{K_0}{M_0} + \frac{4}{45}\frac{\mu_0}{M_0} + \frac{2}{15}\right)\delta_{ij}\delta_{kl} + \left(-\frac{4}{15}\frac{\mu_0}{M_0} - \frac{2}{5}\right)\left(\delta_{ik}\delta_{jl} + \delta_{il}\delta_{jk}\right), \tag{22}$$

for $i, j, k, l = 1, 2, 3$, where M_0 is the P-wave modulus defined as $M_0 = K_0 + \frac{4}{3}\mu_0$. When the semi-axis a, in Eq. (2), goes to infinity, the spheroidal particle becomes a cylindrical fiber with $\mathbf{A}_r$ and $\mathbf{B}$ equal to

$$(A_r)_{ijkl} = \frac{1}{b}\left(\frac{3}{8}\frac{K_r^{\mathrm{S}} + \mu_r^{\mathrm{S}}}{M_0} - \frac{1}{4}\frac{K_r^{\mathrm{S}} + \mu_r^{\mathrm{S}}}{\mu_0}\right)\delta_{ij}\delta_{kl} + \frac{1}{b}\left(-\frac{1}{4}\frac{K_r^{\mathrm{S}} + \mu_r^{\mathrm{S}}}{M_0} + \frac{1}{2}\frac{K_r^{\mathrm{S}} + \mu_r^{\mathrm{S}}}{\mu_0}\right)\left(\delta_{ik}\delta_{jl} + \delta_{il}\delta_{jk}\right), \tag{23}$$

$$B_{ijkl} = \left(-\frac{1}{2}\frac{K_0}{M_0} + \frac{1}{12}\frac{\mu_0}{M_0} + \frac{1}{4}\right)\delta_{ij}\delta_{kl} - \left(\frac{1}{2}\frac{\mu_0}{M_0} + \frac{1}{2}\right)\left(\delta_{ik}\delta_{jl} + \delta_{il}\delta_{jk}\right) \tag{24}$$
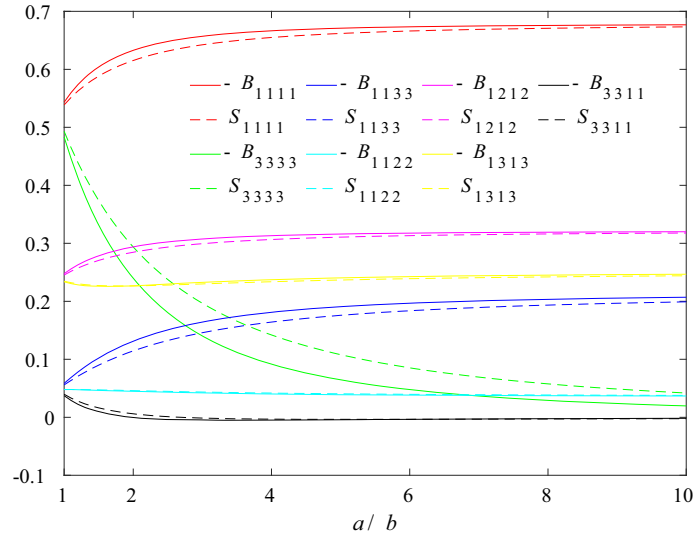
Fig. 1 Comparisons between the coefficient tensor **B** and Eshelby tensor **S** w.r.t. the aspect ratio ($K_0 = 75.2$ GPa, $\mu_0 = 34.7$ GPa)

for $i, j, k, l = 1, 2$, and

$$(A_r)_{1133} = (A_r)_{2233} = \frac{1}{2}\frac{K_r^S - \mu_r^S}{bM_0}, (A_r)_{3311} = (A_r)_{3322} = 0, (A_r)_{1313} = (A_r)_{2323} = \frac{1}{2}\frac{\mu_r^S}{b\mu_0},$$

$$B_{1133} = B_{2233} = -\frac{1}{2}\frac{K_0}{M_0} + \frac{1}{3}\frac{\mu_0}{M_0}, B_{3311} = B_{3322} = 0, B_{1313} = B_{2323} = -\frac{1}{2}.$$

It is noted that under either limiting conditions, i.e., the spheroidal particle becomes a sphere or a cylinder, the coefficient tensor $-\mathbf{B}$ is identical to the well-known Eshelby tensor (see [41,42] for detailed expressions of the Eshelby tensor). For spheroids, the components of tensor $-\mathbf{B}$ is compared with the corresponding components of the Eshelby tensor with the change of aspect ratio in Fig. 1.

The corresponding components in the tensor $-\mathbf{B}$ and the Eshelby tensor are found to be very close between the two limiting conditions, and the deviation is due to the distinct derivation approaches. Different from the Eshelby tensor, which is obtained by integrating the Green's function over the inhomogeneity, the coefficient tensors $\mathbf{A}_r$ and $\mathbf{B}$ in the present paper are derived by solving the generalized Young–Laplace equations and are averaged over the entire *interface*. The components of the tensor $\mathbf{A}_r$ are plotted in Fig. 2 with increasing size of the reinforcement. The components approach zero with increasing size of the reinforcement.

Further, according to Eq. (16), the effective strain in Ω_r can be written as

$$\bar{\boldsymbol{\varepsilon}}_r = \bar{\boldsymbol{\varepsilon}}_0 - \bar{\boldsymbol{\varepsilon}}_r^\lambda = (\mathbf{I} - \mathbf{A}_r) : \bar{\boldsymbol{\varepsilon}}_0 - \mathbf{B} : \boldsymbol{\varepsilon}_r^*. \tag{25}$$

In this section, an interfacial averaged strain discontinuity tensor is derived in order to determine the effective strain in the particle. The corresponding coefficient tensors, $\mathbf{A}_r$ and $\mathbf{B}$, are presented in detail in Appendices 1 and 2 for spheroids, in Eqs. (21), (22) for spheres, and in Eqs. (23), (24) for cylinders. The components of the tensor $\mathbf{A}_r$ exhibit the dependence on the interface elastic stiffness and the dimensions of the particle Ω_r. They decrease as the size of the reinforcement particles increases, leading to a decrease in the interface energy effect. Additionally, when the interface energy effect is neglected, all the components of $\mathbf{A}_r$ become zero. On the other hand, the tensor $\mathbf{B}$ is a constant tensor based on the matrix properties only, which equals to the negative of the Eshelby tensor at limiting conditions. Moreover, the difference between the tensor $-\mathbf{B}$ and the Eshelby tensor for prolate spheroids appears to be negligible.

4 Effective moduli of spheroidal particle-reinforced composites

The strain discontinuity at the interface is established for the composite with a single spheroidal particle inside the otherwise homogeneous effective matrix, and, from which, the strain of the particle is related to the
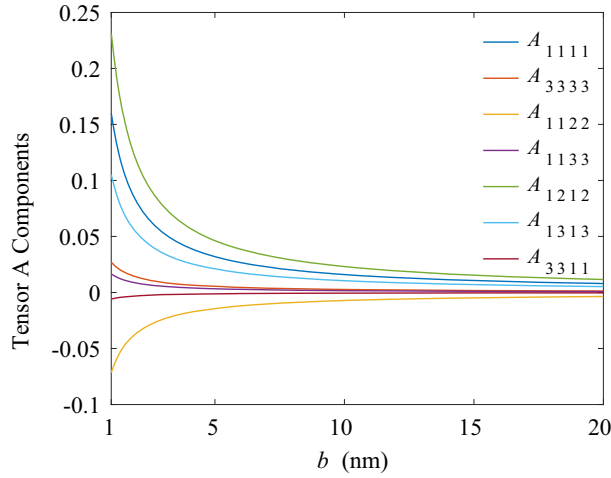
Fig. 2 Components of the coefficient tensor **A** versus the particle size b ($a/b = 3$, $\phi_1 = 0.2$, $K_S = 10$ N/m, $\mu_S = 5$ N/m, $K_0 = 75.2$ GPa, $\mu_0 = 34.7$ GPa)

strain in the matrix. In this section, predictions on the effective elastic stiffness of the multi-particle-reinforced nanocomposites is presented. Now, let us define the effective elastic stiffness tensor $\bar{\mathbf{C}}$ as

$$\bar{\boldsymbol{\sigma}} = \bar{\mathbf{C}} : \bar{\boldsymbol{\varepsilon}}, \tag{26}$$

where $\bar{\boldsymbol{\sigma}}$ and $\bar{\boldsymbol{\varepsilon}}$ are, respectively, the averaged stress and averaged strain tensors of the composite, defined as

$$\bar{\boldsymbol{\sigma}} = \frac{1}{V} \int_V \boldsymbol{\sigma}(\mathbf{x}) d\mathbf{x} = \frac{1}{V} \left[\int_{V_m} \boldsymbol{\sigma}(\mathbf{x}) d\mathbf{x} + \sum_{r=1}^{n} \int_{V_r} \boldsymbol{\sigma}(\mathbf{x}) d\mathbf{x} \right], \tag{27}$$

$$\bar{\boldsymbol{\varepsilon}} = \frac{1}{V} \int_V \boldsymbol{\varepsilon}(\mathbf{x}) d\mathbf{x} = \frac{1}{V} \left[\int_{V_m} \boldsymbol{\varepsilon}(\mathbf{x}) d\mathbf{x} + \sum_{r=1}^{n} \int_{V_r} \boldsymbol{\varepsilon}(\mathbf{x}) d\mathbf{x} \right]. \tag{28}$$

Here, V_m is the volume of matrix, V_r is the total volume of the rth phase particles and n is the total number of particulate phases. Substitution of Eq. (25) into Eq. (10) yields

$$\mathbf{C}_r : \left[(\mathbf{I} - \mathbf{A}_r) : \bar{\boldsymbol{\varepsilon}}_0 - \mathbf{B} : \boldsymbol{\varepsilon}_r^* \right] = \mathbf{C}_0 : \left[(\mathbf{I} - \mathbf{A}_r) : \bar{\boldsymbol{\varepsilon}}_0 - (\mathbf{I} + \mathbf{B}) : \boldsymbol{\varepsilon}_r^* \right]. \tag{29}$$

Then, the eigenstrain $\boldsymbol{\varepsilon}_r^*$ can be derived from Eq. (29):

$$\boldsymbol{\varepsilon}_r^* = \left[(\mathbf{I} + \mathbf{B}) - \mathbf{C}_0^{-1} : \mathbf{C}_r : \mathbf{B} \right]^{-1} : \left[\left(\mathbf{I} - \mathbf{C}_0^{-1} : \mathbf{C}_r \right) : (\mathbf{I} - \mathbf{A}_r) \right] : \bar{\boldsymbol{\varepsilon}}_0. \tag{30}$$

By substituting Eq. (30) into Eq. (28), the averaged strain $\bar{\boldsymbol{\varepsilon}}_r$ of the rth phase particle becomes

$$\bar{\boldsymbol{\varepsilon}}_r = \mathbf{G}_r : \bar{\boldsymbol{\varepsilon}}_0, \tag{31}$$

where $\mathbf{G}_r$ is the local strain concentration tensor defined as:

$$\mathbf{G}_r = \mathbf{I} - \mathbf{A}_r - \mathbf{B} : \left[(\mathbf{I} + \mathbf{B}) - \mathbf{C}_0^{-1} : \mathbf{C}_r : \mathbf{B} \right]^{-1} : \left[\left(\mathbf{I} - \mathbf{C}_0^{-1} : \mathbf{C}_r \right) : (\mathbf{I} - \mathbf{A}_r) \right]. \tag{32}$$

In addition, from Eqs. (28) and (31), we arrive at

$$\bar{\boldsymbol{\varepsilon}}_r = \mathbf{N}_r : \bar{\boldsymbol{\varepsilon}}, \tag{33}$$

where $\mathbf{N}_r$ is the global strain concentration tensor and takes the form:

$$\mathbf{N}_r = \mathbf{G}_r : \left[\phi_m \mathbf{I} + \sum_{r=1}^{n} \phi_r \mathbf{G}_r \right]^{-1}. \tag{34}$$

Here, ϕ_m is the volume fraction of the matrix and ϕ_r is the volume fraction of the rth phase particles. Subsequently, the effective stiffness tensor becomes

$$\bar{\mathbf{C}} = \mathbf{C}_0 + \sum_{r=1}^{n} \phi_r \left(\mathbf{C}_r - \mathbf{C}_0 \right) : \mathbf{N}_r. \tag{35}$$

Based on the interfacial strain discontinuity tensor in the previous section, the effective elastic stiffness is derived following the classical homogenization procedures in the micromechanical framework. Note that the present work considers the particle interactions indirectly. Thus, inaccuracies are induced in the effective stiffness, particularly for composite materials with high particle concentrations. The direct inter-particle interactions were considered by Ju and Chen [9,10], and they showed higher-order estimation of the effective properties, which provide higher accuracy for the composite with high particle concentrations. To provide more accurate solutions at higher particle concentration, future work can be carried out by considering the inter-particle interactions in the present framework.

5 Nanomechanics examples and discussions

In previous sections, a nanomechanics framework is formulated to predict the effective elastic moduli of spheroidal particle-reinforced multi-phase nanocomposites. The formulation is based on the assumption made by Mori and Tanaka on the elastic fields in the matrix surrounding each reinforcement particle [7,8,43]. Different from the classical micromechanical frameworks, the effect of the interface energy on the effective stiffness tensor is considered, and the *generalized* Young–Laplace equations are solved at the interface to determine the strain field inside the particles. In what follows, nanomechanical homogenization examples are presented to compare our solutions in this paper with the classical micromechanical solutions.

5.1 Analytical solutions of effective moduli for the two-phase spherical-particle-reinforced nanocomposite

Let us consider the simplest case of a two-phase spherical-particle-reinforced nanocomposite. Assume that the matrix and the particles are linear isotropic materials with the elastic stiffness tensors $\mathbf{C}_0$ and $\mathbf{C}_1$, respectively. According to Eq. (35), the effective stiffness tensor can be written as

$$\bar{\mathbf{C}} = \mathbf{C}_0 + \phi_1 \left(\mathbf{C}_1 - \mathbf{C}_0 \right) : \mathbf{N}_1, \tag{36}$$

and the corresponding effective bulk modulus and shear modulus are

$$\bar{K} = K_0 + \frac{\phi_1 \left(K_1 - K_0 \right) \left(3M_0 - 4K_1^S/a \right)}{3M_0 + 3 \left(1 - \phi_1 \right) \left(K_1 - K_0 \right) - 4\phi_1 K_1^S/a}, \tag{37}$$

$$\bar{\mu} = \mu_0 + \frac{15\phi_1 \mu_0 M_0 \left(\mu_1 - \mu_0 \right) - \phi_1 \left(\mu_1 - \mu_0 \right) \left[2 \left(3K_0 + 2\mu_0 \right) K_1^S/a + 12M_0 \mu_1^S/a \right]}{15\mu_0 M_0 + 6 \left(1 - \phi_1 \right) \left(\mu_1 - \mu_0 \right) \left(K_0 + 2\mu_0 \right) - \phi_1 \left[2 \left(3K_0 + 2\mu_0 \right) K_1^S/a + 12M_0 \mu_1^S/a \right]}. \tag{38}$$

Compared with the micromechanical Mori–Tanaka solution, the effective moduli are found to have additional size-dependent terms due to the interface energy effect. As the particle size increases, the size-dependent terms decrease. If the interface energy effect is neglected ($K_1^S = \mu_1^S = 0$), then size-dependent terms vanish and Eqs. (36), (37) reduce to the classical micromechanics solutions [41,42].
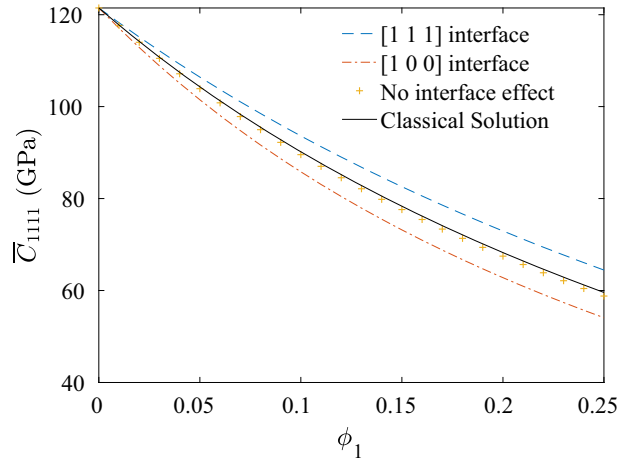
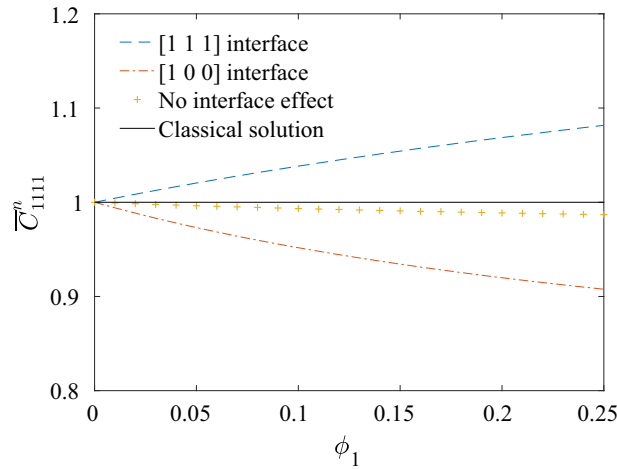**Fig. 3** The effective elastic stiffness $\bar{C}_{1111}$ versus the volume fraction ϕ_1 ($a/b = 5$)

Fig. 4 The normalized effective elastic stiffness $\bar{C}_{1111}$ (w.r.t. the classical micromechanics solution) versus the volume fraction ϕ_1 ($a/b = 5$)

5.2 Numerical solutions of effective elastic stiffness for the two-phase spheroidal particle-reinforced nanocomposite

Next, numerical calculations on the effective elastic stiffness will be presented for the two-phase spheroidal particle-reinforced nanocomposite. Consider an aluminum matrix ($K_0 = 75.2$ GPa, $\mu_0 = 34.7$ GPa) nanocomposite with randomly distributed spheroidal nanovoids. Two sets of interface elastic constants are adopted for illustration. For the (1 1 1) surface, $K_1^S = 12.932$ N/m and $\mu_1^S = -0.3755$ N/m; for the (1 0 0) surface, $K_1^S = -5.457$ N/m and $\mu_1^S = -6.2178$ N/m [12,21,44].

The change of the component $\bar{C}_{1111}$ of the effective stiffness tensor with respect to the volume fraction ϕ of the spheroidal voids is rendered in Figs. 3 and 4. The solutions corresponding to different interface properties are compared with the classical micromechanics solutions. It is observed that as the volume fraction increases, the deviation increases between the solutions with and without the interface effect. Since the total interface area in a composite is proportionally related to the volume fraction of the inhomogeneities, it is reasonable to have larger interface energy effect on the effective elastic stiffness of composites with higher volume fractions.

As the gross interface area is inversely related to the size of the spheroidal particle, the size effect on the effective elastic stiffness is studied. Figures 5 and 6 reveal that the interface energy effect decreases as the particle size increases, and the interface energy has noticeable effect on the effective elastic stiffness for $b < 10$ nm ($a/b = 5$) when the current interface properties are considered. The micromechanical solution of the effective stiffness under our framework (by neglecting the interface energy effect) is also compared
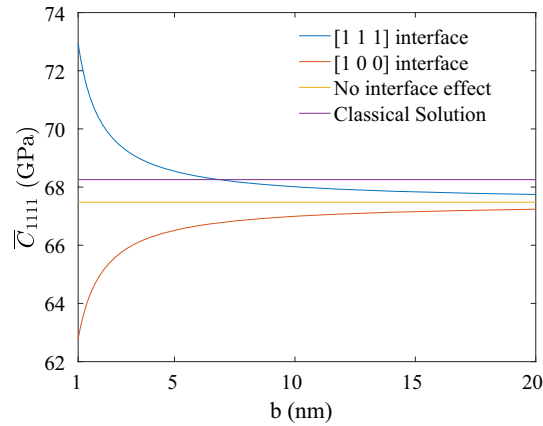
Fig. 5 The effective elastic stiffness $\bar{C}_{1111}$ versus the semi-axis b ($a/b =5$, $\phi_1 = 0.2$)
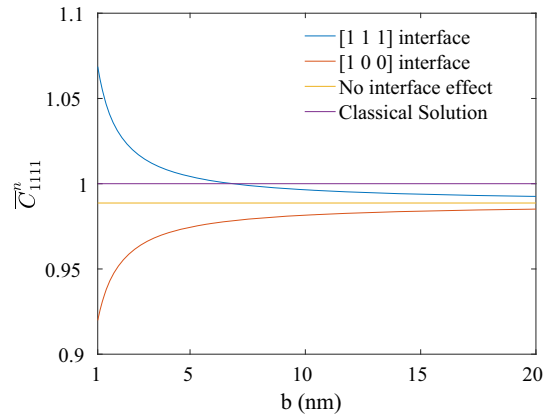

Fig. 6 The normalized effective elastic stiffness $\bar{C}_{1111}$ (w.r.t. the classical micromechanics solution) versus the semi-axis b ($a/b = 5$, $\phi_1 = 0.2$)

with the solution of the classical micromechanics solution. A 1% deviation is observed compared with the micromechanical Mori–Tanaka solution. This is due to the small difference between the coefficient tensor $-\mathbf{B}$ in our formulation and the Eshelby tensor in classical micromechanics formulations for spheroids.

6 Conclusions

(1) The interface energy effect on the elastic behavior of a nanocomposite is discussed. The interface energy effect is regarded as the change of the interface boundary conditions, which is induced by the two-dimensional interface stress at the idealized zero-thickness membrane interface between the inhomogeneity and the matrix. The discontinuous boundary conditions at the interface are presented for spheroidal inhomogeneities.

(2) A nanomechanical framework is formulated to predict the effective moduli of a composite material reinforced by nanosized spheroidal particles. By solving the interfacial discontinuity equations and applying micromechanical homogenization procedures, we relate the effective elastic fields in the inhomogeneities to the effective elastic fields in the matrix. Accordingly, the effective elastic moduli of the nanocomposite are derived.

(3) For illustration purposes, effective moduli for a composite material with spheroidal voids are presented. It is noted that the effective moduli depend upon the dimensions and volume fractions of the spherical inhomogeneities and approach the classical micromechanical results with increasing radius and decreasing volume fractions of the inhomogeneities.

(4) The present paper focuses on the effective performance of nanocomposites in the elastic range. However, for the material composed of the ductile matrix and high elastic stiffness nanoparticles, further research on the elastoplastic behavior is clearly warranted. In our future research, the effective elastoplastic behavior of nanocomposites will be studied systematically.

Appendix 1: The coefficient tensor $\mathbf{A}_r$

The components of the coefficient tensor $\mathbf{A}_r$ for the prolate spheroid in Eq. (2) are

$$(A_r)_{1111} = \frac{1}{8}\frac{K_r^{\mathrm{S}}}{\mu_0}J_1 + \frac{1}{8}\frac{\mu_r^{\mathrm{S}}}{\mu_0}J_2 + \frac{1}{16}\frac{K_r^{\mathrm{S}}}{M_0}J_2 + \frac{1}{16}\frac{\mu_r^{\mathrm{S}}}{M_0}(2J_1 - J_2),$$

$$(A_r)_{1122} = \frac{1}{8}\frac{K_r^{\mathrm{S}}}{\mu_0}J_3 - \frac{1}{8}\frac{\mu_r^{\mathrm{S}}}{\mu_0}J_1 + \frac{1}{16}\frac{K_r^{\mathrm{S}}}{M_0}(2J_1 + J_2) - \frac{1}{16}\frac{\mu_r^{\mathrm{S}}}{M_0}(J_2 + 4J_3),$$

$$(A_r)_{1133} = -\frac{1}{8}\frac{K_r^{\mathrm{S}}}{\mu_0}(J_1 + J_3) + \frac{1}{8}\frac{\mu_r^{\mathrm{S}}}{\mu_0}(J_1 - J_2) + \frac{1}{4}\frac{K_r^{\mathrm{S}}}{M_0}J_1 - \frac{1}{8}\frac{\mu_r^{\mathrm{S}}}{M_0}(J_1 - J_2 - 2J_3),$$

$$(A_r)_{1212} = \frac{1}{8}\frac{K_r^{\mathrm{S}}}{\mu_0}(J_1 - J_3) + \frac{1}{8}\frac{\mu_r^{\mathrm{S}}}{\mu_0}(J_1 + J_2) - \frac{1}{8}\frac{K_r^{\mathrm{S}}}{M_0}J_1 + \frac{1}{8}\frac{\mu_r^{\mathrm{S}}}{M_0}(J_1 + 2J_3),$$

$$(A_r)_{1313} = \frac{1}{8}\frac{K_r^{\mathrm{S}}}{\mu_0}(J_2 + J_3) + \frac{1}{16}\frac{\mu_r^{\mathrm{S}}}{\mu_0}(11J_1 - J_2 + 6J_3) + \frac{1}{8}\frac{K_r^{\mathrm{S}}}{M_0}(J_1 - J_2) - \frac{1}{8}\frac{\mu_r^{\mathrm{S}}}{M_0}(3J_1 - J_2 + 2J_3),$$

$$(A_r)_{3311} = -\frac{1}{8}\frac{K_r^{\mathrm{S}}}{\mu_0}(J_1 + J_3) + \frac{1}{8}\frac{\mu_r^{\mathrm{S}}}{\mu_0}(J_1 - J_2) + \frac{1}{16}\frac{K_r^{\mathrm{S}}}{M_0}(5J_1 + J_2 + 6J_3) - \frac{1}{16}\frac{\mu_r^{\mathrm{S}}}{M_0}(3J_1 - J_2 + 2J_3),$$

$$(A_r)_{3333} = \frac{1}{4}\frac{K_r^{\mathrm{S}}}{\mu_0}(J_1 + J_3) - \frac{1}{4}\frac{\mu_r^{\mathrm{S}}}{\mu_0}(J_1 - J_2) - \frac{1}{8}\frac{K_r^{\mathrm{S}}}{M_0}(J_1 - J_2) + \frac{1}{8}\frac{\mu_r^{\mathrm{S}}}{M_0}(3J_1 - J_2 + 2J_3),$$

where

$$J_1 = \frac{\pi\left[a\left(8a^4 - 2a^2b^2 + 3b^4\right)\sqrt{a^2 - b^2} + b^2\left(-8a^4 - 4a^2b^2 + 3b^4\right)\tanh^{-1}e\right]}{S\left(a^2 - b^2\right)^{5/2}},$$

$$J_2 = \frac{\pi\left[a\left(8a^4 - 42a^2b^2 + 7b^4\right)\sqrt{a^2 - b^2} + b^2\left(24a^4 - 4a^2b^2 + 7b^4\right)\tanh^{-1}e\right]}{S\left(a^2 - b^2\right)^{5/2}},$$

$$J_3 = \frac{\pi\left[a\left(-8a^4 + 10a^2b^2 + b^4\right)\sqrt{a^2 - b^2} + b^2\left(8a^4 - 12a^2b^2 + b^4\right)\tanh^{-1}e\right]}{S\left(a^2 - b^2\right)^{5/2}}.$$

Further, $e = \sqrt{1 - \frac{b^2}{a^2}}$ is the eccentricity, and $S = a\pi b^2\left(1 + \frac{a}{be}\arcsin e\right)$ is the surface area of the prolate spheroid.

Appendix 2: The coefficient tensor B

The components of the coefficient tensor $\mathbf{B}$ for the prolate spheroids in Eq. (2) are

$$B_{1111} = -\frac{1}{2}I_1 - \frac{K_0}{\mu_0}I_2 + \frac{1}{6}\frac{\mu_0}{M_0}(3I_1 - 8I_2),$$

$$B_{1122} = -\frac{1}{6}(I_1 - 4I_2) - \frac{K_0}{\mu_0}I_2 + \frac{1}{6}\frac{\mu_0}{M_0}I_1,$$

$$B_{1133} = \frac{2}{3}(I_1 - I_2) - \frac{K_0}{\mu_0}I_2 + \frac{2}{3}\frac{\mu_0}{M_0}(I_1 - 2I_2),$$

$$B_{1212} = -\frac{1}{3}(I_1 + 2I_2) + \frac{1}{3}\frac{\mu_0}{M_0}(I_1 - 4I_2),$$

$$B_{1313} = -(I_1 + I_3) - \frac{4}{3}\frac{\mu_0}{M_0}(I_1 - I_2),$$

$$B_{3311} = \frac{2}{3}(I_1 - I_2) - \frac{K_0}{\mu_0}(I_1 - I_2 + I_3) + \frac{2}{3}\frac{\mu_0}{M_0}I_3,$$

$$B_{3333} = -\frac{4}{3}(I_1 - I_2) - \frac{K_0}{\mu_0}(I_1 - I_2 + I_3) - \frac{4}{3}\frac{\mu_0}{M_0}I_3,$$

where

$$I_1 = \frac{\pi a^2 b \left[b\left(a^2 - 10b^2\right)\sqrt{a^2 - b^2} + \left(25a^4 - 24a^2b^2 + 8b^4\right)\tan^{-1}\frac{\sqrt{a^2-b^2}}{b} \right]}{S\left(a^2 - b^2\right)^{5/2}},$$

$$I_2 = \frac{\pi a^2 b \left[b\sqrt{a^2 - b^2} + \left(a^2 - 2b^2\right)\tan^{-1}\frac{\sqrt{a^2-b^2}}{b} \right]}{S\left(a^2 - b^2\right)^{3/2}},$$

$$I_3 = \frac{\pi b \left[b^3\left(7a^2 + 2b^2\right)\sqrt{a^2 - b^2} + a^2\left(-24a^4 + 23a^2b^2 - 8b^4\right)\tan^{-1}\frac{\sqrt{a^2-b^2}}{b} \right]}{S\left(a^2 - b^2\right)^{5/2}}.$$

References

1. Wood, J.: The top ten advances in materials science. Mater. Today **11**, 40–45 (2008)
2. Giannelis, E.P.: Polymer layered silicate nanocomposites. Adv. Mater. **8**, 29–35 (1996)
3. Ray, S.S., Okamoto, M.: Polymer/layered silicate nanocomposites: a review from preparation to processing. Prog. Polym. Sci. **28**, 1539–1641 (2003)
4. Eshelby, J.D.: The determination of the elastic field of an ellipsoidal inclusion, and related problems. Proc. R. Soc. Lond. A **241**, 376–396 (1957)
5. Eshelby, J.D.: Elastic inclusion and inhomogeneities. Prog. Solid Mech. **2**, 89–140 (1961)
6. Withers, P.J., Stobbs, W.M., Pedersen, O.B.: The application of the Eshelby method of internal stress determination to short fibre metal matrix composites. Acta Metall. **37**(11), 3061–3084 (1989)
7. Mori, T., Tanaka, K.: Average stress in matrix and average elastic energy of materials with misfitting inclusions. Acta Metall. **21**, 571–574 (1973)
8. Weng, G.J.: Some elastic properties of reinforced solids, with special reference to isotropic ones containing spherical inclusions. Int. J. Eng. Sci. **22**, 845–856 (1984)
9. Ju, J.W., Chen, T.M.: Micromechanics and effective moduli of elastic composites containing randomly dispersed ellipsoidal inhomogeneities. Acta Mech. **103**, 103–121 (1994a)
10. Ju, J.W., Chen, T.M.: Effective elastic moduli of two-phase composites containing randomly dispersed spherical inhomogeneities. Acta Mech. **103**, 123–144 (1994b)
11. Gibbs, J.W.: The Scientific Papers of J. Willard Gibbs, vol. 1. Longmans, Green and Company, London (1906)
12. Duan, H.L., Wang, J.X., Huang, Z.P., Karihaloo, B.L.: Size-dependent effective elastic constants of solids containing nano-inhomogeneities with interface stress. J. Mech. Phys. Solids **53**, 1574–1596 (2005)
13. Cammarata, R.C.: Surface and interface stress effects on interfacial and nanostructured materials. Mater. Sci. Eng. A **237**, 180–184 (1997)
14. Walpole, L. J.: A coated inclusion in an elastic medium. In Mathematical Proceedings of the Cambridge Philosophical Society, vol. 83, no. 3, pp. 495–506. Cambridge University Press, Cambridge (1978)
15. Mikata, Y., Taya, M.: Stress field in and around a coated short fiber in an infinite matrix subjected to uniaxial and biaxial loadings. J. Appl. Mech. **52**, 19–24 (1985)
16. Qiu, Y.P., Weng, G.J.: Elastic moduli of thickly coated particle and fiber-reinforced composites. J. Appl. Mech. **58**, 388–398 (1991)
17. Herve, E., Zaoui, A.: N-layered inclusion-based micromechanical modelling. Int. J. Eng. Sci. **31**, 1–10 (1993)
18. Duan, H.L., Wang, J., Huang, Z.P., Luo, Z.Y.: Stress concentration tensors of inhomogeneities with interface effects. Mech. Mater. **37**(7), 723–736 (2005)
19. Shuttleworth, R.: The surface tension of solids. Proc. Phys. Soc. Sect. A **63**, 444 (1950)

20. Gurtin, M.E., Murdoch, A.I.: theory of elastic material surfaces. Arch. Ration. Mech. Anal. **57**, 291–323 (1975)
21. Miller, R.E., Shenoy, V.B.: Size-dependent elastic properties of nanosized structural elements. Nanotechnology **11**, 139 (2000)
22. Dingreville, R., Qu, J., Cherkaoui, M.: Surface free energy and its effect on the elastic behavior of nano-sized particles, wires and films. J. Mech. Phys. Solids **53**, 1827–1854 (2005)
23. Wang, Z.Q., Zhao, Y.P., Huang, Z.P.: The effects of surface tension on the elastic properties of nano structures. Int. J. Eng. Sci. **48**, 140–150 (2010)
24. Sharma, P., Ganti, S., Bhate, N.: Effect of surfaces on the size-dependent elastic state of nano-inhomogeneities. Appl. Phys. Lett. **82**, 535–537 (2003)
25. Sharma, P., Ganti, S.: Size-dependent Eshelby's tensor for embedded nano-inclusions incorporating surface/interface energies. J. Appl. Mech. **71**, 663–671 (2004)
26. Kushch, V.I., Mogilevskaya, S.G., Stolarski, H.K., Crouch, S.L.: Elastic interaction of spherical nanoinhomogeneities with Gurtin–Murdoch type interfaces. J. Mech. Phys. Solids **59**(9), 1702–1716 (2011)
27. Kushch, V.I., Mogilevskaya, S.G., Stolarski, H.K., Crouch, S.L.: Elastic fields and effective moduli of particulate nanocomposites with the Gurtin–Murdoch model of interfaces. Int. J. Solids Struct. **50**(7–8), 1141–1153 (2013)
28. Shodja, H.M., Hashemian, B.: Variational bounds and overall shear modulus of nano-composites with interfacial damage in anti-plane couple stress elasticity. Int. J. Damage Mech. (2019). https://doi.org/10.1177/1056789519856934
29. Alemi, B., Shodja, H.M.: Effective shear modulus of solids reinforced by randomly oriented-/aligned-elliptic multi-coated nanofibers in micropolar elasticity. Compos. Part B Eng. **143**, 197–206 (2018)
30. Heidarhaei, M., Shariati, M., Eipakchi, H.R.: Effect of interfacial debonding on stress transfer in graphene reinforced polymer nanocomposites. Int. J. Damage Mech. **27**(7), 1105–1127 (2018)
31. Rostamiyan, Y., Ferasat, A.: High-speed impact and mechanical strength of ZrO_2/polycarbonate nanocomposite. Int. J. Damage Mech. **26**(7), 989–1002 (2017)
32. Fan, M., Zhang, Y.M., Xiao, Z.M.: The interface effect of a nano-inhomogeneity on the fracture behavior of a crack and the nearby edge dislocation. Int. J. Damage Mech. **26**(3), 480–497 (2017)
33. Voyiadjis, G.Z., Kattan, P.I.: Fundamental aspects for characterization in continuum damage mechanics. Int. J. Damage Mech. **28**(2), 200–218 (2019)
34. Chen, T., Chiu, M.S., Weng, C.N.: Derivation of the generalized Young–Laplace equation of curved interfaces in nanoscaled solids. J. Appl. Phys. **100**, 074308 (2006)
35. Bottomley, D.J., Ogino, T.: Alternative to the Shuttleworth formulation of solid surface stress. Phys. Rev. B. **63**, 165412 (2001)
36. Mi, C., Jun, S., Kouris, D.A., Kim, S.Y.: Atomistic calculations of interface elastic properties in noncoherent metallic bilayers. Phys. Rev. B. **63**(7), 075425 (2008)
37. Pahlevani, L., Shodja, H.M.: Surface and interface effects on torsion of eccentrically two-phase fcc circular nanorods: determination of the surface/interface elastic properties via an atomistic approach. J. Appl. Mech. **78**(1), 011011 (2011)
38. Shodja, H.M., Pahlevani, L.: Surface/interface effect on the scattered fields of an anti-plane shear wave in an infinite medium by a concentric multi-coated nanofiber/nanotube. Eur. J. Mech. A Solid **32**, 21–31 (2012)
39. Shodja, H.M., Enzevaee, C.: Surface characterization of face-centered cubic crystals. Mech. Mater. **129**, 15–22 (2019)
40. Zhang, W.X., Wang, T.J., Chen, X.: Effect of surface/interface stress on the plastic deformation of nanoporous materials and nanocomposites. Int. J. Plast. **26**(7), 957–975 (2010)
41. Mura, T.: Micromechanics of Defects in Solids. Springer, Berlin (2013)
42. Qu, J., Cherkaoui, M.: Fundamentals of Micromechanics of Solids. Wiley, Hoboken (2006)
43. Weng, G.J.: The theoretical connection between Mori–Tanaka's theory and the Hashin–Shtrikman–Walpole bounds. Int. J. Eng. Sci. **28**, 1111–1120 (1990)
44. Sharma, P., Dasgupta, A.: Average elastic fields and scale-dependent overall properties of heterogeneous micropolar materials containing spherical and cylindrical inhomogeneities. Phys. Rev. B. **66**, 224110 (2002)